

# Metabolomics-Guided Discovery, Isolation, Structure Elucidation, and Bioactivity of Myropeptins C–E from *Myrothecium inundatum*

Annika Jagels, Donovan A. Adpressa, Elizabeth N. Kaweesa, Mark McCauley, Benjamin Philmus, James A. Strother, and Sandra Loesgen\*



Cite This: *J. Nat. Prod.* 2023, 86, 1723–1735



Read Online

ACCESS |



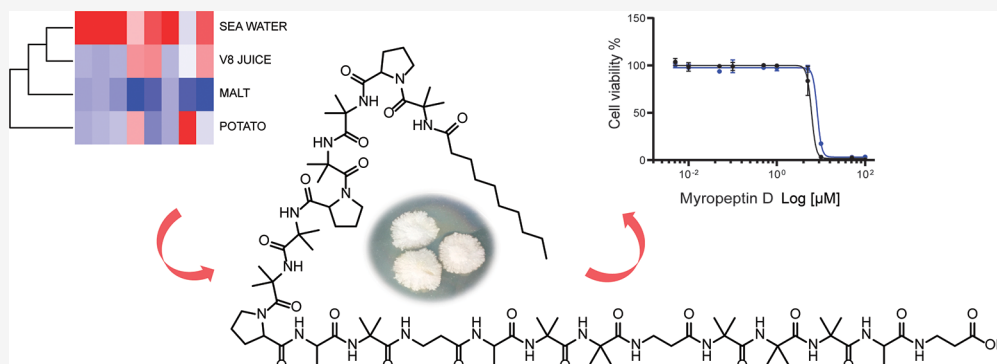
Metrics & More



Article Recommendations



Supporting Information



**ABSTRACT:** The saprotrophic filamentous fungus *Myrothecium inundatum* represents a chemically underexplored ascomycete with a high number of putative biosynthetic gene clusters in its genome. Here, we present new linear lipopeptides from nongenetic gene activation experiments using nutrient and salt variations. Metabolomics studies revealed four myropeptins, and structural analyses by NMR, HRMS, Marfey's analysis, and ECD assessment for their helical properties established their absolute configuration. A myropeptin biosynthetic gene cluster in the genome was identified. The myropeptins exhibit general nonspecific toxicity against all cancer cell lines in the NCI-60 panel, larval zebrafish with  $EC_{50}$  concentrations of 5–30  $\mu\text{M}$ , and pathogenic bacteria and fungi (MICs of 4–32  $\mu\text{g}/\text{mL}$  against multidrug-resistant *S. aureus* and *C. auris*). *In vitro* hemolysis, cell viability, and ionophore assays indicate that the myropeptins target mitochondrial and cellular membranes, inducing cell depolarization and cell death. The toxic activity is modulated by the length of the lipid side chain, which provides valuable insight into their structure–activity relationships.

The fungal genus *Myrothecium* (family Stachybotriaceae, order Hypocreales) includes a diversity of endophytic, saprophytic, and pathogenic species.<sup>1,2</sup> *Myrothecium inundatum* was first described by Tode in 1790,<sup>1</sup> but is chemically underexplored, although a small number of secondary metabolites, including bioactive di- and triterpenes, were recently reported from an endolichenic *M. inundatum* strain.<sup>3</sup> The genome of *M. inundatum* CBS120646 was sequenced and made publicly available by the Department of Energy Joint Genome Institute (JGI, <https://mycocosm.jgi.doe.gov/Myrin1/Myrin1.home.html>).<sup>4</sup> It contains over 80 annotated biosynthetic gene clusters (BGCs), suggesting many dormant secondary metabolites compared with the small number of metabolites that have been discovered thus far. Generally, most BGCs are not expressed under common laboratory conditions,<sup>5</sup> but exposing a strain to varied biotic and abiotic culture conditions, including different media nutrients, temperatures, light, pH, or cocultivation, can activate repressed BGCs.<sup>6–8</sup> Here, by changing the culture conditions we isolated highly toxic lipopeptides: myropeptin A<sub>1</sub>, previously described from an *M. roridum* strain,<sup>9</sup> and three new myropeptins with a

single amino acid change or different length fatty acid chain. We report the isolation, structure elucidation, and *in vitro* and *in vivo* activity of myropeptins E–C (1–3) and the full spectroscopic assignment and bioactivity of the known myropeptin A<sub>1</sub> (4)<sup>9</sup> from *M. inundatum*. In addition, we identify a putative biosynthetic gene cluster containing a 20-module nonribosomal peptide synthetase (NRPS).

## RESULTS AND DISCUSSION

*M. inundatum* was cultured in four media conditions: malt extract-peptone (M2), tomato juice (V8), potato extract-dextrose (PDA), and starch-yeast-peptone-seawater (SYP-SW). The metabolites produced were detected with high-

Received: February 20, 2023

Published: July 6, 2023



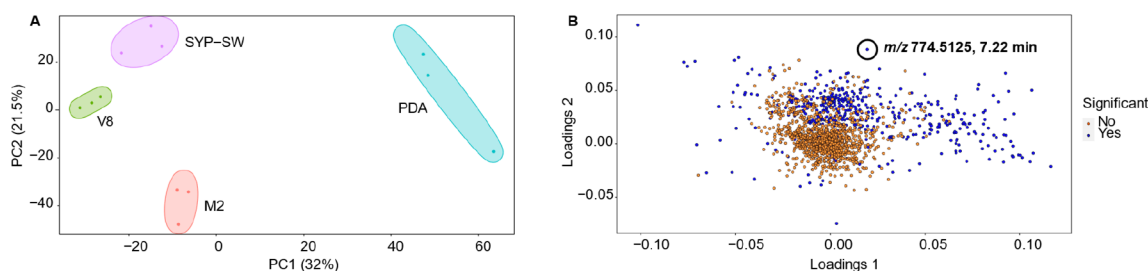


**Figure 1.** (A) PCA scores plot and (B) PCA loadings plot of *M. inundatum* metabolome after cultivation for 2 weeks, 26 °C, in different media (M2, V8, PDA, and SYP-SW,  $n = 3$ , 95% confidence interval of normalized  $m/z$  intensities from LC-HRMS, positive ionization mode). PCA loading plot (B) depicts one of the significantly distinct (ANOVA, accompanied by Fisher's least significant difference test and an FDR correction) features found in the SYP-SW extract.

resolution LC-MS and analyzed with multivariate statistics and principal component analysis (PCA). The PDA-derived metabolome was the most distinct from that produced in the media M2, V8, and SYP-SW (Figure 1A); however this was due to few, low-abundant mass spectrometric features. We focused on the metabolome derived from seawater-based media, which revealed significantly different and more abundant metabolites (Figure 1B).

The fungal metabolome, grown in the SYP-SW medium, exhibited unique and highly abundant mass spectrometric features with large  $m/z$  values at four different retention times. Related mass features eluted at specific times (7.2/7.3 min  $m/z$  774.51 and 1052.61; 7.8 min  $m/z$  774.51 and 1066.62; 8.0/7.9 min  $m/z$  802.54 and 1052.61; 8.6 min  $m/z$  802.54 and 1066.62 (Figure 2).

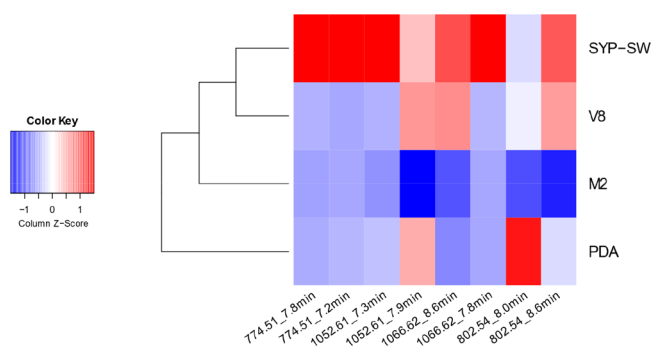


**Figure 2.** Heatmap visualization abundance of mass spectrometric features for *M. inundatum* cultivated in SYP-SW, V8, M2, and PDA media for 2 weeks, 26 °C. The blue color represents low abundance, and the red color represents high abundance.

**Structure Elucidation.** Four compounds of *M. inundatum* cultured in SYP-SW medium were targeted for isolation based on the mass spectrometric features from the metabolomic profiling. The structure determination of the lipopeptides was performed using a combination of MS/MS and extensive NMR analyses. Myropeptin C (**1**) was isolated as a white, amorphous powder. Electrospray ionization coupled with high-resolution mass spectrometry (ESI-HRMS) confirmed the molecular mass and formula of myropeptin C (**1**) of  $C_{87}H_{148}N_{20}O_{22}$  (Figure 4B). Additionally, isotope labeling experiments with  $^{15}N$ -ammonium chloride resulted in the incorporation of 20  $^{15}N$  atoms, corroborating the presence of 20 amino acids in total (Figure 3C).

The MS<sup>2</sup> patterns of the two in-source fragments from positive ionization resembled peptides. Indeed, 10 b-ions were

produced upon fragmentation of the  $m/z$  1052 fragment, and neutral losses derived from respective amino acids were assigned (Figure 4A). The  $m/z$  774 portion was more challenging to analyze, but several b-ions, internal b-ions, and an a-ion were detected (Figure 4B).

The  $^1H$  NMR data in DMF- $d_7$  revealed 17 amide protons from 7.28 to 8.70 ppm. From the recorded  $^{13}C$  NMR spectrum, 19 carbonyl carbons from 172.2 to 177.0 ppm and 11 aliphatic nonprotonated carbons from 56.3 to 56.9 ppm were observed (Table 1, Figure S22). HMBC correlations between a bulk of methyl protons (1.42–1.60 ppm) and carbons between 56.3 and 56.9 ppm confirmed the presence of 11 Aib residues (Figure 5A, Figures S15–S19). Analysis of protons ranging from 3.31 to 4.38 ppm (Table 1, Figure S21) in combination with 2D-NMR data including HSQC (Figure S23), TOCSY (Figure S24), and HMBC (Figures S25 and S26) suggested that **1** contains three alanine (Ala), three proline (Pro), and two  $\beta$ -alanine ( $\beta$ ala) residues, supported by the HRMS fragmentation pattern (Figure 4). The number of methylene groups ( $^1H$  1.22–1.37 ppm,  $^{13}C$  22.6–35 ppm), their TOCSY interactions, and one HMBC correlation to a carbonyl group indicated a saturated fatty acid chain in the molecule (Figure 5A).

MS<sup>2</sup> fragmentation of the  $m/z$  774 in-source fragment ion resulted in the generation of (internal) b-ions (Figure 4B), and accurate  $m/z$  values of respective fragments confirmed the presence of a decanoyl ( $C_{10}$ ) chain attached to the C-terminus. NOESY correlations verified the sequence of the 20-mer:  $C_{10}$ -Aib-Pro-Aib-Aib-Pro-Aib-Aib-Pro-Ala-Aib- $\beta$ ala-Ala-Aib-Aib- $\beta$ ala-Aib-Aib-Aib-Ala- $\beta$ ala (Figure 5A).

Compound **2** featured a similar unique set of in-source fragmentation ions with  $m/z$  values of 774.5138 and 1066.6269 (7.8 min) but shared the same  $m/z$  774 fragment as seen in **1** (Supporting Information, Figures S2 and S5). The second fragment mass increase of 14 Da from  $m/z$  1052 to  $m/z$  1066 suggested a congener with an additional methyl(ene) group. Indeed, analysis of the MS<sup>2</sup> fragmentation pattern of  $m/z$  1066 uncovered a different  $b_{10}$ -ion (Supporting Information, Figure S5). Instead of a Pro-Ala fragment ( $m/z$  169.0976) found in myropeptin C,  $m/z$  183.1129 was detected for Pro-Aib. All other neutral losses were identical to **1**, and hence, the compound was named myropeptin D (**2**). The molecular formula of **2** was determined by ESI-HRMS to be  $C_{88}H_{150}N_{20}O_{22}$ ,  $m/z$  918.5544,  $[M - 2H]^{2-}$  calcd 918.5544 (Supporting Information, Figure S2). As expected, protons from 4.10 to 4.22 ppm were found in the  $^1H$  NMR and HSQC spectra (Table 2, Supporting Information, Figure S29) for two Ala moieties instead of three, while the three Pro residues

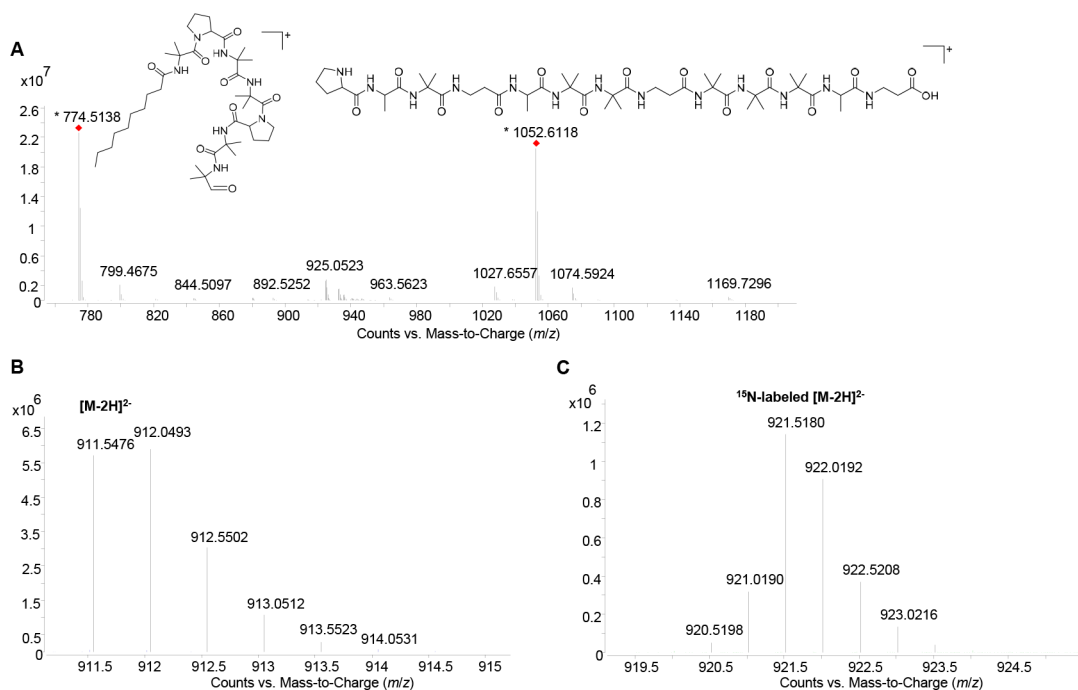


**Figure 3.** (A) MS<sup>1</sup> spectra of myropeptin C (**1**), in positive ionization mode, (B) in negative ionization mode, and (C) in negative ionization mode after <sup>15</sup>N-labeling. (The doubly charged ion is shown in B and C).

remained. NOESY and HMBC correlations (Supporting Information, Figures S31–S34) supported the peptide sequence to be C<sub>10</sub>-Aib-Pro-Aib-Aib-Pro-Aib-Aib-Pro-Aib-Aib-βala-Ala-Aib-Aib-βala-Aib-Aib-Aib-Ala-βala (Figure S5B).

The remaining two related peptides that eluted at *t*<sub>R</sub> 8.0 and 8.6 min shared the characteristic MS<sup>2</sup> feature of *m/z* 802 and unique mass fragments of *m/z* 1052 and *m/z* 1066, respectively. An increase of 28 Da from the *m/z* 774 feature of myropeptins C and D to *m/z* 802 suggested the addition of two methyl(ene) groups. With no remarkable changes in the <sup>1</sup>H NMR and identical neutral amino acid losses in the MS<sup>2</sup> compared to **1** and **2**, we hypothesized the additional methylene groups to be in the fatty acid moiety. Indeed, the MS<sup>2</sup> fragmentation pattern (Supporting Information, Figure S6) as well as the observed 11 aliphatic carbon NMR shifts, instead of nine, supports a dodecanoyl (C<sub>12</sub>) chain (Table 3, Supporting Information, Figure S36). The new peptide with a molecular formula of C<sub>90</sub>H<sub>154</sub>N<sub>20</sub>O<sub>22</sub> (HRMS (ESI) *m/z* 932.5701, [M – 2H]<sup>2–</sup> calcd 932.5701, Supporting Information, Figure S3) and sequence of C<sub>12</sub>-Aib-Pro-Aib-Aib-Pro-Aib-Aib-Pro-Aib-Aib-βala-Ala-Aib-Aib-βala-Aib-Aib-Aib-Ala-βala was named myropeptin E (**3**).

Lastly, based on MS<sup>2</sup> and 2D-NMR analyses, the peptide eluting at 8.0 min with the mass spectroscopic in-source fragments *m/z* 802 and 1052 was determined to be myropeptin A<sub>1</sub><sup>9</sup> (**4**) with the molecular formula of C<sub>89</sub>H<sub>152</sub>N<sub>20</sub>O<sub>22</sub> (Figure S4). The structural assignment and sequence were supported by MS<sup>2</sup> (Figure S7), NMR experiments including <sup>15</sup>N-HSQC, and selected HMBC correlations (Table S2, Figures S8–S20) to be C<sub>12</sub>-Aib-Pro-Aib-Aib-Pro-Aib-Aib-Pro-Ala-Aib-βala-Ala-Aib-Aib-βala-Aib-Aib-Aib-Ala-βala. Myropeptin A<sub>1</sub> was first reported by Yoshimura and co-workers in 2019 as an inseparable mixture together with myropeptin A<sub>2</sub> from *M. roridum*.<sup>9</sup> Here we add detailed spectroscopic data for purified myropeptin A<sub>1</sub>, and we also provide expanded bioactivity testing. For all four

myropeptins, we employed advanced Marfey's analysis<sup>10</sup> and determined the amino acids to be L-configured; additionally the presence of βala and Aib was confirmed (Figure S41). With chemical shift differences between the β- and the γ-carbons (ΔδC<sub>β</sub>–δC<sub>γ</sub>) between 2.7 and 3.5 ppm for the three Pro residues, their *trans* conformation was deduced.<sup>11</sup>

Peptides featuring a large number of Aib residues tend to form helical structures.<sup>12,13</sup> We recorded circular dichroism (CD) spectra for the myropeptins (**1–4**), which display helical behavior with a positive band around 190 nm and negative bands at 208 and 230 nm (Figure 6). Specifically, we have an indication of a 3<sub>10</sub>-helix in solution, as reported for myropeptin A<sub>1</sub> (**4**)<sup>9</sup> and gichigamin A,<sup>14</sup> based on the weak positive band at 192 nm and the negative band at 207 nm accompanied by a shoulder band at 225 nm (absorption ratio *R* = mdeg<sub>225</sub>/mdeg<sub>207</sub> of 0.4).<sup>15</sup>

**Genome Analysis of *Myrothecium inundatum* CBS 120646.** The genome of *M. inundatum* CBS 120646 was sequenced, assembled, and made publicly available by JGI (project ID: 1019495, genome version 01).<sup>4</sup> After annotation of the genome with fungiSMASH (version 5.1.2)<sup>16</sup> we identified 12 NRPS-PKS hybrid clusters, with six matching a lipopeptide made by an NRPS and type-I PKS hybrid (T1PKS) (cf. Supporting Information, Figure S42). Specifically, scaffold\_2\_c8–region 1 (region on contig edge, total of 121,819 nt) encoded a T1PKS cluster (782,386–788,169, total, 5508 nt, excluding introns) adjacent to a 20-amino-acid-encoding NRPS module 782,386–788,169 (total: 5508 nt, excluding introns) (Figure 7) that matched the structures of the myropeptins, which contain 20 amino acids.

The PKS is putatively responsible for the formation of the decanoyl and dodecanoyl lipid chains and is a highly reducing iterative PKS with the domain order KS-AT-DH-KR-ACP. The PKS does not encode an enoyl reductase (ER) domain, and we were unable to identify an ER in proximity to the BGC, and we propose that ER activity is supplied by another protein

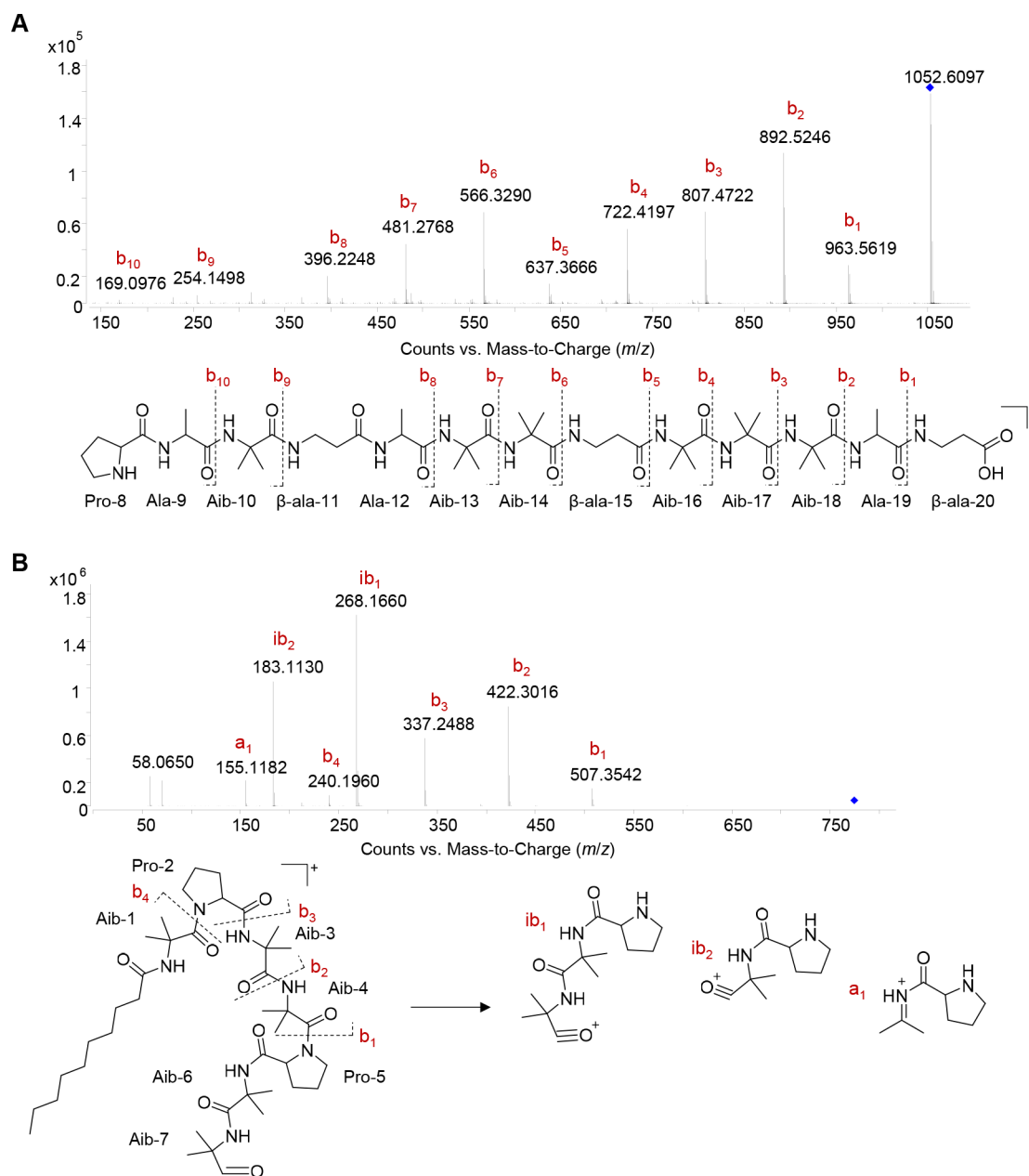


**Figure 4.** (A) QTOF-MS<sup>2</sup> spectra of myropeptin C (**1**) of in-source fragment 1052.6097 [M + H]<sup>+</sup> and (B) in-source fragment 774.5138 [M + H]<sup>+</sup>, collision-induced dissociation (35 eV); dashed lines show generated b-ions.

encoded at disparate genomic loci. The fatty acid is likely transferred from the PKS to the initial T domain of the NRPS and then coupled with the downstream Aib residue. There are 19 elongation modules consisting of C-A-T domains and a C-terminal condensation domain, similar to previously described fungal NRPS.<sup>18,19</sup> The adenylation (A) domains can be used to infer the amino acid specificity (Stachelhaus prediction, Figure 7, Table S3)<sup>20,21</sup> via NRPSpredictor2<sup>22</sup> (integrated into fungiSMASH version 5.1.2) (Figure 7A). Pro were predicted with high confidence, but no predictions were possible at several positions where βala or Ala was found. Iva is predicted to be incorporated by most modules (1, 3, 4, 6, 7, 10, 13, 14, 16, and 17); however, we observed Aib being incorporated into the myropeptins at these positions. Interestingly, the Stachelhaus code predicting the amino acid loading at position 9 is unique compared to the others that encode for Aib and Ala

(Figure 7B), and this is responsible for the sequence differences between myropeptins C/A<sub>1</sub> and D/E.

**Biological Activity. Antimicrobial Activity.** Lipopeptides **1–4** were active against *Enterococcus faecium*, *Staphylococcus aureus* (methicillin-susceptible, methicillin-resistant, and multi-drug-resistant), and *Candida auris* (Table 4, Supporting Information, Table S4). Myropeptin A<sub>1</sub> (**4**) exhibited the most potent activity with an MIC value of 4 μg/mL (2 μM) against *S. aureus* and *C. auris*, myropeptins C and D (**1** and **2**) demonstrated moderate MIC values of 16 μg/mL (8 μM), and myropeptin E showed less activity, with MIC values from 4 to 16 μg/mL (2–8 μM) (Figure S43). Total growth inhibition was observed for myropeptins C, D, and A<sub>1</sub> around 64–128 μg/mL (32–64 μM), while myropeptin E induced a stunted growth phenotype (cf. Supporting Information, Figure S43).

Table 1. NMR Data of Myropeptin C (1) in DMF-*d*<sub>7</sub> (600 and 150 MHz,  $\delta$  in ppm, \* signal overlapped, \*\* signal not detected)

residue	$\delta^{13}\text{C}$ , type	$\delta^{\text{H}}$ , mult., (J in Hz)	residue	$\delta^{13}\text{C}$ , type	$\delta^{\text{H}}$ , mult., (J in Hz)	residue	$\delta^{13}\text{C}$ , type	$\delta^{\text{H}}$ , mult., (J in Hz)
C <sub>10</sub>	13.8, CH <sub>3</sub>	0.87, t (6.8)	Aib <sub>6</sub> , NH		7.62, s*	Aib <sub>14</sub> , NH		7.62, s*
C <sub>9</sub>	22.6, CH <sub>2</sub>	1.22–1.37*	$\alpha$	56.9, C		$\alpha$	56.8, C	
C <sub>8</sub>	31.9, CH <sub>2</sub>	1.22–1.37*	$\beta_1$	23.3, CH <sub>3</sub>	1.63, m	$\beta_1$	23.5–27.7, CH <sub>3</sub>	1.47, m*
C <sub>7</sub>	29.3, CH <sub>2</sub>	1.22–1.37*	$\beta_2$	23.4, CH <sub>3</sub>	1.51, m*	$\beta_2$	23.5–27.7, CH <sub>3</sub>	1.47, m*
C <sub>6</sub>	29.5, CH <sub>2</sub>	1.22–1.37*	C=O	177.0, C		C=O	175.7, C	
C <sub>5</sub>	29.4, CH <sub>2</sub>	1.22–1.37*	Aib <sub>7</sub> , NH		8.02, s	$\beta\text{ala}_{15}$ , NH		7.71, s
C <sub>4</sub>	29.2, CH <sub>2</sub>	1.22–1.37*	$\alpha$	56.8, C		$\alpha$	37.9, CH <sub>2</sub>	2.45; 2.40, m
C <sub>3</sub>	24.5, CH <sub>2</sub>	1.61*	$\beta_1$	23.4, CH <sub>3</sub>	1.59, m*	$\beta$	36.3, CH <sub>2</sub>	3.63; 3.31, m
C <sub>2</sub>	35.0*, CH <sub>2</sub>	2.36; 2.33, m	$\beta_2$	25.9, CH <sub>3</sub>	1.44, m*	C=O	172.7, C	
C <sub>1</sub> , C=O	173.5, C		C=O	173.5, C		Aib <sub>16</sub> , NH		8.29, s
Aib <sub>1</sub> , NH		8.70, s	Pro <sub>8</sub> $\alpha$	63.3, CH	4.38, m	$\alpha$	56.5, C	
$\alpha$	56.3, C		$\beta$	28.9*, CH <sub>2</sub>	2.28; 1.81, m	$\beta_1$	23.5–27.7, CH <sub>3</sub>	1.42–1.60, m*
$\beta_1$	25.3, CH <sub>3</sub>	1.53, m	$\gamma$	25.7, CH <sub>2</sub>	1.94, m	$\beta_2$	23.5–27.7, CH <sub>3</sub>	1.42–1.60, m*
$\beta_2$	23.4, CH <sub>3</sub>	1.46, m	$\delta$	48.8, CH <sub>2</sub>	4.04; 3.73, m	C=O	175.7, C	
C=O	174.0, C		C=O	173.4, C		Aib <sub>17</sub> , NH		8.56, s
Pro <sub>2</sub> $\alpha$	64.1, CH	4.19, m	Ala <sub>9</sub> , NH		7.92, s	$\alpha$	56.8, C	
$\beta$	28.8, CH <sub>2</sub>	2.29; 1.70, m	$\alpha$	50.7, CH	4.16, m	$\beta_1$	23.5–27.7, CH <sub>3</sub>	1.42–1.60, m*
$\gamma$	25.3, CH <sub>2</sub>	1.99; 1.92, m	$\beta$	16.6, CH <sub>3</sub>	1.45, m	$\beta_2$	23.5–27.7, CH <sub>3</sub>	1.42–1.60, m*
$\delta$	48.9, CH <sub>2</sub>	3.95; 3.45, m	C=O	173.1, C		C=O	176.2, C	
C=O	172.2, C		Aib <sub>10</sub> , NH		7.52, s*	Aib <sub>18</sub> , NH		7.93, s*
Aib <sub>3</sub> , NH		7.62, s*	$\alpha$	56.8, C		$\alpha$	56.8, C	
$\alpha$	56.9, C		$\beta_1$	26.0, CH <sub>3</sub>	1.49, m	$\beta_1$	23.5–27.7, CH <sub>3</sub>	1.42–1.60, m*
$\beta_1$	23.3, CH <sub>3</sub>	1.60, m	$\beta_2$	26.0, CH <sub>3</sub>	1.51, m	$\beta_2$	23.5–27.7, CH <sub>3</sub>	1.42–1.60, m*
$\beta_2$	23.5–27.7, CH <sub>3</sub>	1.50, m	C=O	175.0, C		C=O	174.9, C	
C=O	176.2, C		$\beta\text{ala}_{11}$ , NH		7.28, t (6.0)	Ala <sub>19</sub> , NH		7.79, d, (7.9)
Aib <sub>4</sub> , NH		7.94, s*	$\alpha$	36.6, CH <sub>2</sub>	2.47; 2.41, m	$\alpha$	49.7, CH	4.19, m
$\alpha$	56.6, C		$\beta$	36.4, CH <sub>2</sub>	3.57; 3.33, m	$\beta$	17.1, CH <sub>3</sub>	1.42, m
$\beta_1$	23.4, CH <sub>3</sub>	1.46, m	C=O	172.5, C		C=O	173.0, C	
$\beta_2$	23.4, CH <sub>3</sub>	1.59, m	Ala <sub>12</sub> , NH		8.27, s	$\beta\text{ala}_{20}$ , NH		7.52, s*
C=O	173.7, C		$\alpha$	51.5, CH	4.09, m	$\alpha$	35.0*, CH <sub>2</sub>	2.54; 2.51, m
Pro <sub>5</sub> $\alpha$	64.3, CH	4.19, m	$\beta$	16.6, CH <sub>3</sub>	1.40, m	$\beta$	36.3, CH <sub>2</sub>	3.41; 3.40, m
$\beta$	28.9*, CH <sub>2</sub>	2.27; 1.74, m	C=O	174.5, C		C=O	** , C	
$\gamma$	25.8, CH <sub>2</sub>	1.98; 1.93, m	Aib <sub>13</sub> , NH		8.49, s			
$\delta$	48.9, CH <sub>2</sub>	3.76; 3.89, m	$\alpha$	56.6, C				
C=O	172.5, C		$\beta_1$	23.5–27.7, CH <sub>3</sub>	1.42–1.60, m*			
			$\beta_2$	23.5–27.7, CH <sub>3</sub>	1.42–1.60, m*			
			C=O	174.6, C				

**In Vitro Cytotoxicity.** Myropeptin A<sub>1</sub> (4) was cytotoxic to HCT116 human colon carcinoma and MDA-MB-231 human breast cancer cells with average IC<sub>50</sub> values of 1  $\mu\text{M}$  to both cell lines (Figure 8).<sup>23</sup> Myropeptins C (1), D (2), and E (3) exhibited slightly higher IC<sub>50</sub> values ranging from 5 to 11  $\mu\text{M}$ . Notably, the dose–response curves for these lipopeptides were extremely steep, especially for myropeptin A<sub>1</sub>, a characteristic also seen in the National Cancer Institute’s (NCI) 60 cell line panel (Supporting Information, Figure S44). Myropeptin A<sub>1</sub> (4) exhibited strong inhibitory activity against all tested cancer cell lines in the five-dose assay, conducted on two different occasions. Only four leukemia cell lines and the ovarian cell line OVCAR-8 are less responsive to myropeptin A<sub>1</sub> with LC<sub>50</sub> values of >16  $\mu\text{M}$  (cf. Supporting Information, Figure S44).

**In Vitro Hemolytic Activity and in Vivo Toxicity (Zebrafish Assay).** To study the interactions of lipopeptides with membranes, hemolysis experiments were carried out with sheep erythrocytes, and the release of hemoglobin was used to quantify the membrane-damaging properties.<sup>9</sup> Interestingly, the dodecanoyl-containing myropeptins E (3) and A<sub>1</sub> (4) exhibited lower IC<sub>50</sub> values (2.0 and 1.5  $\mu\text{M}$ , respectively) compared to those of the decanoyl myropeptins C (1) and D

(2) (7 and 10  $\mu\text{M}$ , respectively) (Figure 9A). We hypothesized that the length of the fatty acid chain modulates hemolysis, which was supported by *in vivo* toxicity data in a zebrafish assay. Here, compound 4 with the C<sub>12</sub> fatty acid chain induced 100% mortality in zebrafish embryos at 10  $\mu\text{M}$ , while compound 1 with a C<sub>10</sub> fatty acid side chain required a 5-fold higher concentration (50  $\mu\text{M}$ ) for the same effect (Figure 9), which agrees with the observed hemolytic effects of 1–4. Notably, in both assays, the dose response curves were exceptionally steep and similar to the cytotoxicity assay curves.

**Ionophoric Activity.** Due to the amphipathic nature and helical structures of the myropeptins, their effect on membrane stability was examined. In our Fluo-4-AM calcium imaging assay,<sup>24</sup> myropeptin A<sub>1</sub> (4) acts as a Ca<sup>2+</sup>-ionophore, as does the positive control ionomycin (Figure 10). Ionomycin induced Ca<sup>2+</sup>-influx starting at 1  $\mu\text{M}$  with a rapid increase of fluorescence onset at higher concentration (4  $\mu\text{M}$ ), which resembles the IC<sub>50</sub> value of 3.8  $\mu\text{M}$  (Supporting Information, Figure S45). Myropeptin A<sub>1</sub> (4) causes slight Ca<sup>2+</sup>-influx at 4  $\mu\text{M}$  and rapid influx at 8  $\mu\text{M}$ , cells swell instantly once perfusion with 4 begins and many cells rupture; at 16  $\mu\text{M}$ , we most likely observe the lysis of cells, which results in the loss of

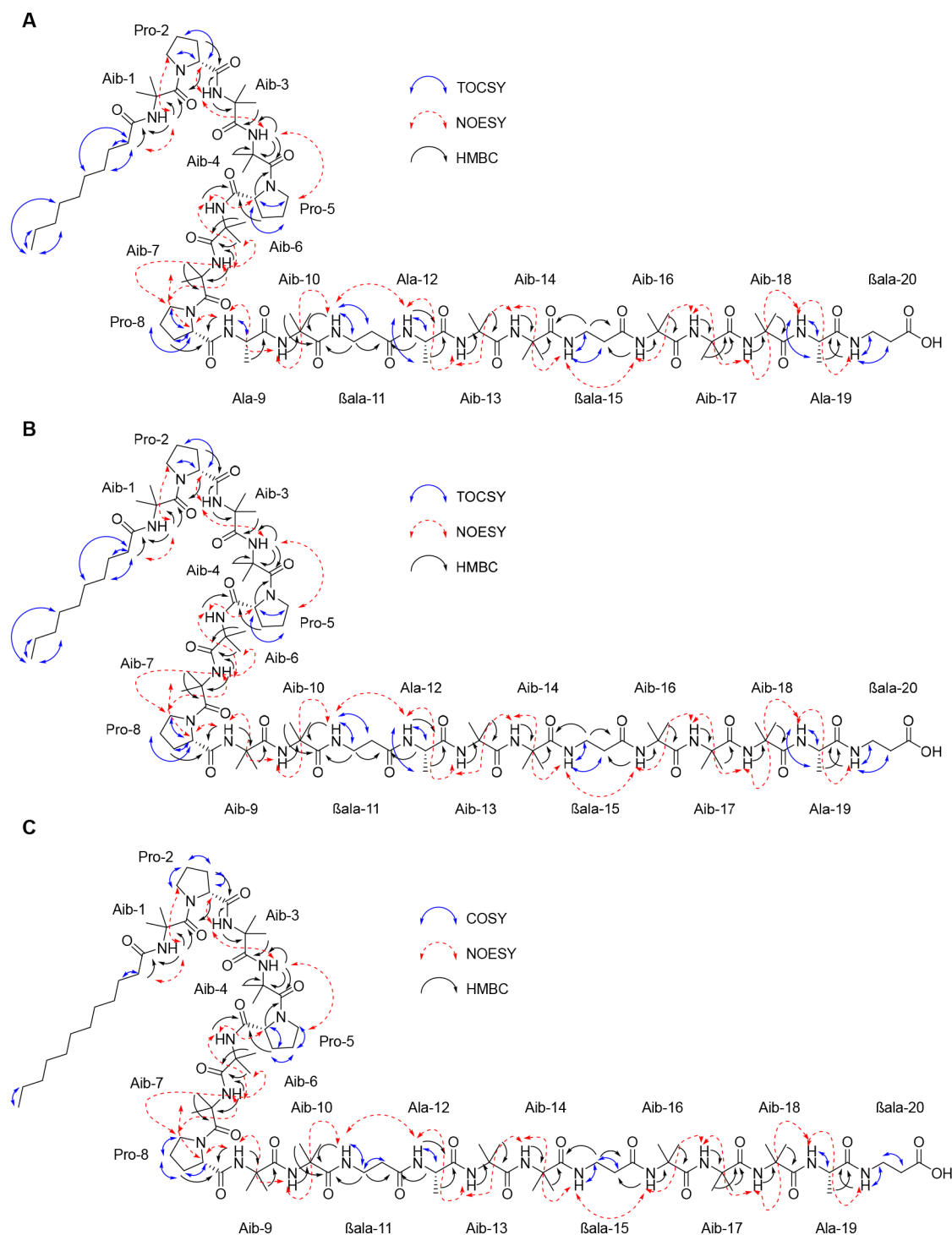


**Figure 5.** (A–C) Key 2D NMR correlations (TOCSY, COSY, NOESY, and HMBC) of myropeptins C–E (1–3) in  $\text{DMF-}d_7$ .

Fluo-4, which might explain the rapid onset but also decline in fluorescence (Figure 10B, Figure S46).

**Influence on the Mitochondrial Membrane Potential.** Gichigamin A, a peptaibol rich in  $\beta$ ala and Aib residues, and its synthetic derivatives selectively disrupt mitochondrial function after penetrating intact cells.<sup>14</sup> Therefore, an intracellular target might be affected first before pore formation in the cellular membrane is lethal. A transmembrane potential ( $\Delta\Psi_m$ ) across the mitochondrial membrane generates ATP, and a voltage-indicating fluorescent dye can be used to visualize mitochondrial health.<sup>25</sup> Cells were incubated and imaged with 4,

MitoOrange, and CMTMRos dye. The mitochondrial uncoupling reagent carbonyl cyanide-*p*-trifluoromethoxyphenylhydrazone (FCCP) was used as a positive control. Untreated cells (0.1% DMSO) are healthy, and MitoOrange dye accumulates in the mitochondria. FCCP-treated cells exhibit less dye accumulation and show signs of apoptosis, such as membrane blebbing. Cells treated with 1  $\mu\text{M}$  myropeptin A<sub>1</sub> (4) also show less dye accumulation comparable to FCCP (50  $\mu\text{M}$ ), but no membrane blebbing or other signs of apoptosis (Supporting Information, Figure S47).

Table 2. NMR Data of Myropeptin D (2) in DMF-*d*<sub>7</sub> (600 and 150 MHz,  $\delta$  in ppm, \* signal overlapped, \*\* signal not detected)

residue	$\delta^{13}\text{C}$ , type	$\delta^1\text{H}$ , mult., (J in Hz)	residue	$\delta^{13}\text{C}$ , type	$\delta^1\text{H}$ , mult., (J in Hz)	residue	$\delta^{13}\text{C}$ , type	$\delta^1\text{H}$ , mult., (J in Hz)
C <sub>10</sub>	13.6, CH <sub>3</sub>	0.88, t (6.9)	Aib <sub>6</sub> , NH		7.58, s	Aib <sub>14</sub> , NH		7.61, s*
C <sub>9</sub>	22.6, CH <sub>2</sub>	1.22–1.37*	$\alpha$	57.0, C		$\alpha$	56.8, C	
C <sub>8</sub>	31.9, CH <sub>2</sub>	1.22–1.37*	$\beta_1$	23.4, CH <sub>3</sub>	1.51, m	$\beta_1$	23.3–27.7, CH <sub>3</sub>	1.40–1.63, m*
C <sub>7</sub>	29.3, CH <sub>2</sub>	1.22–1.37	$\beta_2$	23.8, CH <sub>3</sub>	1.51, m	$\beta_2$	23.3–27.7, CH <sub>3</sub>	1.40–1.63, m*
C <sub>6</sub>	29.5, CH <sub>2</sub>	1.22–1.37**	C=O	176.9, C		C=O	175.7, C	
C <sub>5</sub>	29.4, CH <sub>2</sub>	1.22–1.37*	Aib <sub>7</sub> , NH		8.02, s	$\beta\text{ala}_{15}$ , NH		7.68, s
C <sub>4</sub>	29.2, CH <sub>2</sub>	1.22–1.37*	$\alpha$	56.7, C		$\alpha$	37.9, CH <sub>2</sub>	2.43; 2.41, m
C <sub>3</sub>	25.3, CH <sub>2</sub>	1.62, m	$\beta_1$	23.3–27.7, CH <sub>3</sub>	1.40–1.63, m*	$\beta$	36.3, CH <sub>2</sub>	3.61; 3.31, m
C <sub>2</sub>	34.9, CH <sub>2</sub>	2.36; 2.33, m	$\beta_2$	23.3–27.7, CH <sub>3</sub>	1.40–1.63, m*	C=O	172.5, C	
C <sub>1</sub> , C=O	174.4, C		C=O	173.4, C		Aib <sub>16</sub> , NH		8.29, s
Aib <sub>1</sub> , NH		8.68, s	Pro <sub>8</sub>	63.9, CH	4.22, m	$\alpha$	56.5, C	
$\alpha$	56.3, C		$\beta$	28.8, CH <sub>2</sub>	2.28; 1.81, m	$\beta_1$	23.3–27.7, CH <sub>3</sub>	1.40–1.63, m*
$\beta_1$	26.0, CH <sub>3</sub>	1.53, m	$\gamma$	25.7, CH <sub>2</sub>	1.94, m	$\beta_2$	23.3–27.7, CH <sub>3</sub>	1.40–1.63, m*
$\beta_2$	23.9, CH <sub>3</sub>	1.46, m	$\delta$	48.7, CH <sub>2</sub>	4.03; 3.73, m	C=O	175.6, C	
C=O	174.7, C		C=O	174.1, C		Aib <sub>17</sub> , NH		8.54, s
Pro <sub>2</sub> $\alpha$	64.1, CH	4.20, m	Aib <sub>9</sub> , NH		7.87, s	$\alpha$	56.8, C	
$\beta$	28.8, CH <sub>2</sub>	2.29; 1.70, m	$\alpha$	56.6, C		$\beta_1$	23.3–27.7, CH <sub>3</sub>	1.40–1.63, m*
$\gamma$	26.0, CH <sub>2</sub>	1.99; 1.92, m	$\beta_1$	23.3–27.7, CH <sub>3</sub>	1.40–1.63, m*	$\beta_2$	23.3–27.7, CH <sub>3</sub>	1.40–1.63, m*
$\delta$	48.9, CH <sub>2</sub>	3.95; 3.45, m	$\beta_2$	23.3–27.7, CH <sub>3</sub>	1.40–1.63, m*	C=O	176.1, C	
C=O	172.2, C		C=O	176.0, C		Aib <sub>18</sub> , NH		7.92, s*
Aib <sub>3</sub> , NH		7.63, s*	Aib <sub>10</sub> , NH		7.50, s*	$\alpha$	56.8, C	
$\alpha$	57.0, C		$\alpha$	56.8, C		$\beta_1$	23.3–27.7, CH <sub>3</sub>	1.40–1.63, m*
$\beta_1$	23.5, CH <sub>3</sub>	1.60, m	$\beta_1$	23.3–27.7, CH <sub>3</sub>	1.40–1.63, m*	$\beta_2$	23.3–27.7, CH <sub>3</sub>	1.40–1.63, m*
$\beta_2$	23.3–27.7, CH <sub>3</sub>	1.40–1.63, m*	$\beta_2$	23.3–27.7, CH <sub>3</sub>	1.40–1.63, m*	C=O	174.9, C	
C=O	176.1, C		C=O	175.0, C		Ala <sub>19</sub> , NH		7.79, s
Aib <sub>4</sub> , NH		7.93, s*	$\beta\text{ala}_{11}$ , NH		7.32, s	137	49.7, CH	4.20, m
$\alpha$	56.7, C		$\alpha$	36.5, CH <sub>2</sub>	2.47; 2.41, m	139	17.1, CH <sub>3</sub>	1.40, m
$\beta_1$	23.3–27.7, CH <sub>3</sub>	1.40–1.63, m*	$\beta$	36.2, CH <sub>2</sub>	3.32, m	C=O	173.0, C	
$\beta_2$	23.3–27.7, CH <sub>3</sub>	1.40–1.63, m*	C=O	172.5, C		$\beta\text{ala}_{20}$ , NH		7.51, s*
C=O	173.6, C		Ala <sub>12</sub> , NH		8.26, d (4.5)	$\alpha$	34.5, CH <sub>2</sub>	2.47, m
Pro <sub>5</sub>	64.3, CH	4.19, m	$\alpha$	51.5, CH	4.10, m	$\beta$	35.8, CH <sub>2</sub>	3.32; 3.54, m
$\beta$	28.9, CH <sub>2</sub>	2.27; 1.74, m	$\beta$	16.5, CH <sub>3</sub>	1.40, m	C=O	** , C	
$\gamma$	25.7, CH <sub>2</sub>	1.98; 1.93, m*	C=O	174.5, C				
$\delta$	48.8, CH <sub>2</sub>	3.76; 3.90, m	Aib <sub>13</sub> , NH		8.54, s			
C=O	172.4, C		$\alpha$	56.7, C				
			$\beta_1$	23.3–27.7, CH <sub>3</sub>	1.40–1.63, m*			
			$\beta_2$	23.3–27.7, CH <sub>3</sub>	1.40–1.63, m*			
			C=O	174.5, C				

**Flow Cytometry-Based Apoptosis Detection.** To determine if the myropeptins induce apoptosis in SK-Mel-5 cells, a flow cytometry approach with FITC-annexin V and propidium iodide (PI) was used.<sup>26</sup> Annexin V labeling indicates both early and late stages of apoptosis, whereas PI-stained cells are late phase apoptotic or necrotic. We applied concentrations lower or around the IC<sub>50</sub> value, e.g., 0.5–0.7  $\mu\text{M}$ , and did not observe any FITC or PI signal increase or cellular changes after 3–4 h of incubation (Supporting Information, Figure S48). Only at concentrations of 1  $\mu\text{M}$  or higher can some signs of early apoptosis be observed for cells treated with 4, similarly to the control of 5  $\mu\text{M}$  camptothecin. At this concentration, annexin-PI staining is observed after an incubation time of 10 min, accompanied with a ballooning cell morphology (similarly to gichigamin A-treated cells).<sup>14</sup> Taken together with the cell membrane disruption seen in the Fluo-4 AM assay at concentrations >4  $\mu\text{M}$  of 4, apoptosis may be a downstream event but is likely not the cause of cell death for these fast acting lipopeptides.

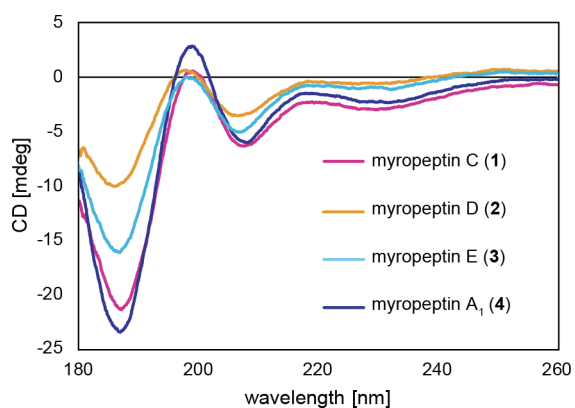
## EXPERIMENTAL SECTION

**General Experimental Procedures.** Myropeptins C, D, and A<sub>1</sub> 1D and 2D NMR spectra were recorded at 600 MHz for <sup>1</sup>H NMR and 150 MHz for <sup>13</sup>C NMR at 318 K on a Bruker Avance III HD instrument equipped with a 1.7 mm TCI cryoprobe. Myropeptin E 1D and 2D NMR spectra were recorded at 800 MHz for <sup>1</sup>H NMR (equipped with a 5 mm TCI cryoprobe) and 201 MHz for <sup>13</sup>C NMR on a Bruker Avance III spectrometer (Billerica, MA, USA) with DMF-*d*<sub>7</sub> as the solvent and internal standard at 318 K in a 1.5 mm HTS probe. The solvent signals were referenced to  $\delta_{\text{H}} = 2.92$  ppm and  $\delta_{\text{C}} = 163.15$  ppm. Optical rotations were determined on a PerkinElmer 341 polarimeter at the sodium D line (589 nm), 20 s integration time, and rotations were averaged over six integration periods. CD was measured with a J-1500 spectropolarimeter (Jasco, Oklahoma City, OK, USA) at 100  $\mu\text{g}/\text{mL}$  in acetonitrile/water (1/1, v/v) at 20 °C from 180 to 260 nm with a 1 s DIT, 0.1 nm data interval, 1.00 nm bandwidth, and 50 nm scanning speed for 2 accumulations.

High-resolution LC-MS experiments for metabolomic profiling were conducted on an Agilent 1290 Infinity II series UPLC coupled to an Agilent 6546 QTOF mass spectrometer with an electrospray ionization (ESI) source (Agilent Technologies, Santa Clara, CA, USA). Chromatography was performed using a Kinetex C<sub>18</sub> column

Table 3. NMR Data of Myropeptin E (3) in DMF-*d*<sub>7</sub> (800 and 201 MHz,  $\delta$  in ppm, \* signal overlapped)

residue	$\delta^{13}\text{C}$ , type	$\delta^1\text{H}$ , mult., (J in Hz)	residue	$\delta^{13}\text{C}$ , type	$\delta^1\text{H}$ , mult., (J in Hz)	residue	$\delta^{13}\text{C}$ , type	$\delta^1\text{H}$ , mult., (J in Hz)
C <sub>12</sub>	13.9, CH <sub>3</sub>	0.88, t (7.2)	Aib <sub>6</sub> , NH		7.57, s	Aib <sub>14</sub> , NH		7.63, s
C <sub>11</sub>	22.7, CH <sub>2</sub>	1.24–1.36*	$\alpha$	57.1, C		$\alpha$	56.9, C	
C <sub>10</sub>	32.0*, CH <sub>2</sub>	1.24–1.36*	$\beta_1$	23.5, CH <sub>3</sub>	1.64, s	$\beta_1$	23.5–27.2, CH <sub>3</sub>	1.42–1.51, m*
C <sub>9</sub>	29.3, CH <sub>2</sub>	1.24–1.36*	$\beta_2$	23.6–27.2, CH <sub>3</sub>	1.42–1.51, m*	$\beta_2$	23.5–27.2, CH <sub>3</sub>	1.42–1.51, m*
C <sub>8</sub>	29.6, CH <sub>2</sub>	1.24–1.36*	C=O	176.3, C		C=O	175.5, C	
C <sub>7</sub>	29.5, CH <sub>2</sub>	1.24–1.36*	Aib <sub>7</sub> , NH		7.97, s	$\beta_{\text{ala}_{15}}$ , NH		7.70, t (6.0)
C <sub>6</sub>	29.3, CH <sub>2</sub>	1.24–1.36*	$\alpha$	57.0, C		$\alpha$	37.8, CH <sub>2</sub>	2.29, 2.30, m
C <sub>5</sub>	29.4, CH <sub>2</sub>	1.24–1.36*	$\beta_1$	23.4, CH <sub>3</sub>	1.59, s	$\beta$	36.5, CH <sub>2</sub>	3.37, m*
C <sub>4</sub>	29.3, CH <sub>2</sub>	1.24–1.36*	$\beta_2$	23.6–27.2	1.42–1.51, m*	C=O	172.7, C*	
C <sub>3</sub>	25.2, CH <sub>2</sub>	1.62, m*	C=O	173.4, C		Aib <sub>16</sub> , NH		8.53, s
C <sub>2</sub>	34.8, CH <sub>2</sub>	2.34; 2.37, m	Pro <sub>8</sub> , $\alpha$	63.9, CH <sub>2</sub>	4.25, m	$\alpha$	56.7, C	
C <sub>1</sub> , C=O	174.0, C		$\beta$	29.1, CH <sub>2</sub>	2.28; 1.75, m*	$\beta_1$	23.5–27.2, CH <sub>3</sub>	1.42–1.51, m*
Aib <sub>1</sub> , NH		8.66, s	$\gamma$	26.1, CH <sub>2</sub>	1.99; 1.92, m*	$\beta_2$	23.5–27.2, CH <sub>3</sub>	1.42–1.51, m*
$\alpha$	56.5, C		$\delta$	48.9, CH	3.96; 3.77, m	C=O	175.5, C	
$\beta_1$	25.9, CH <sub>3</sub>	1.54, s	C=O	173.7, C		Aib <sub>17</sub> , NH		8.78, s
$\beta_2$	24.4, CH <sub>3</sub>	1.42–1.51, m*	Aib <sub>9</sub> , NH		7.84, s	$\alpha$	56.7, C	
C=O	174.7, C		$\alpha$	56.8, CH		$\beta_1$	23.5–27.2, CH <sub>3</sub>	1.42–1.51, m*
Pro <sub>2</sub> , $\alpha$	64.2, CH	4.21, m	$\beta_1$	23.5–27.2, CH <sub>3</sub>	1.42–1.51, m*	$\beta_2$	23.5–27.2, CH <sub>3</sub>	1.42–1.51, m*
$\beta$	28.9, CH <sub>2</sub>	2.28; 1.71, m	$\beta_2$	23.5–27.2, CH <sub>3</sub>	1.42–1.51, m*	C=O	175.8, C	
$\gamma$	26.2, CH <sub>2</sub>	1.99; 1.92, m*	C=O	175.8, C		Aib <sub>18</sub> , NH		7.87, s
$\delta$	49.0, CH <sub>2</sub>	3.87; 3.46, m	Aib <sub>10</sub> , NH		7.47, s	$\alpha$	56.9, C	
C=O	172.3, C		$\alpha$	56.9, C		$\beta_1$	23.5–27.2, CH <sub>3</sub>	1.42–1.51, m*
Aib <sub>3</sub> , NH		7.70, s	$\beta_1$	23.5–27.2, CH <sub>3</sub>	1.42–1.51, m*	$\beta_2$	23.5–27.2, CH <sub>3</sub>	1.42–1.51, m*
$\alpha$	57.1, C		$\beta_2$	23.5–27.2, CH <sub>3</sub>	1.42–1.51, m*	C=O	174.8, C	
$\beta_1$	23.6, CH <sub>3</sub>	1.61, s	C=O	175.0, C		Ala <sub>19</sub> , NH		7.76, d (7.9)
$\beta_2$	27.8, CH <sub>3</sub>	1.42–1.51, m*	$\beta_{\text{ala}_{11}}$ , NH		7.41, t (5.6)	$\alpha$	49.8, CH	4.20, m
C=O	176.1, C		$\alpha$	36.5, CH <sub>2</sub>	2.49; 2.42*	$\beta$	17.4, CH <sub>3</sub>	1.40, m*
Aib <sub>4</sub> , NH		7.93, s	$\beta$	36.3, CH <sub>2</sub>	3.37*	C=O	172.9, C	
$\alpha$	56.9, C		C=O	172.4, C		$\beta_{\text{ala}_{20}}$ , NH		7.50, t (5.8)
$\beta_1$	23.5–23.8, CH <sub>3</sub>	1.55, s	Ala <sub>12</sub> , NH		8.41, s	$\alpha$	34.6, CH <sub>2</sub>	2.42, m*
$\beta_2$	23.5–27.2, CH <sub>3</sub>	1.42–1.51, m*	$\alpha$	51.3, CH	4.16, m	$\beta$	35.7, CH <sub>2</sub>	3.37, m*
C=O	173.7, C		$\beta$	16.9, CH <sub>3</sub>	1.39, m*	C=O	176.3, C	
Pro <sub>5</sub> , $\alpha$	64.4, CH <sub>2</sub>	4.21, m	C=O	174.2, C				
$\beta$	29.0, CH <sub>2</sub>	2.28; 1.75, m*	Aib <sub>13</sub> , NH		8.72, s			
$\gamma$	26.1, CH <sub>2</sub>	1.99; 1.92, m*	$\alpha$	56.7, C				
$\delta$	49.0, CH	3.77; 3.89, m*	$\beta_1$	23.5–27.2, CH <sub>3</sub>	1.42–1.51, m*			
C=O	172.7, C*		$\beta_2$	23.5–27.2, CH <sub>3</sub>	1.42–1.51, m*			
			C=O	174.6, C				

Figure 6. Circular dichroism (CD) spectra of lipopeptides 1–4 in acetonitrile/water (1/1, v/v) at 100  $\mu\text{g}/\text{mL}$ .

(50  $\times$  2.1 mm, 2.6, Phenomenex, Torrance, CA, USA), the oven temperature was set to 40  $^{\circ}\text{C}$ , and the sample injection volume was 5  $\mu\text{L}$ . A binary gradient consisting of MeCN (eluent A) and water (eluent B) (both +0.1% formic acid (FA)) at a constant flow rate of

500  $\mu\text{L}/\text{min}$  was used. The gradient was applied as follows: 0–0.25 min, 10% A; 10.00 min, 95% A; 13.00 min, 95% A; 13.1 min, 10% A; 15.00 min 10% A. For data acquisition and subsequent qualitative analysis, MassHunter software (Agilent Technologies, Santa Clara, CA, USA) was used. All parameters regarding the QTOF are listed in the Supporting Information, Table S5.

**Data Treatment, Processing, and Statistical Analysis for Metabolomics.** The obtained raw data files were first converted into mzML format using the msconvert tool provided by ProteoWizard.<sup>27</sup> The following multistage processing of the data was performed using MZmine 2<sup>28</sup> to obtain a feature list (respective mass-to-charge ratios with corresponding retention times and peak areas). Processing steps and applied parameters are given in the Supporting Information Table S1. The processed feature list was exported into a CSV file for statistical analysis by using the export tool in MZmine 2. Features from the different growth media were normalized (missing values set to zero) and analyzed with PCA in RStudio.<sup>29</sup> PCA loadings were tested for significance using ANOVA, accompanied by a Fishers LSD test and FDR correction. Heatmap visualization of mass spectrometric feature abundances was averaged from triplicates, normalized to the highest and lowest intensities, and z-scored, using ggplot2 v3.4.0.<sup>30</sup>

**Fungal Strain and Culture Conditions.** The fungal strain *M. inundatum* CBS 120646 was purchased from the Westerdijk Fungal

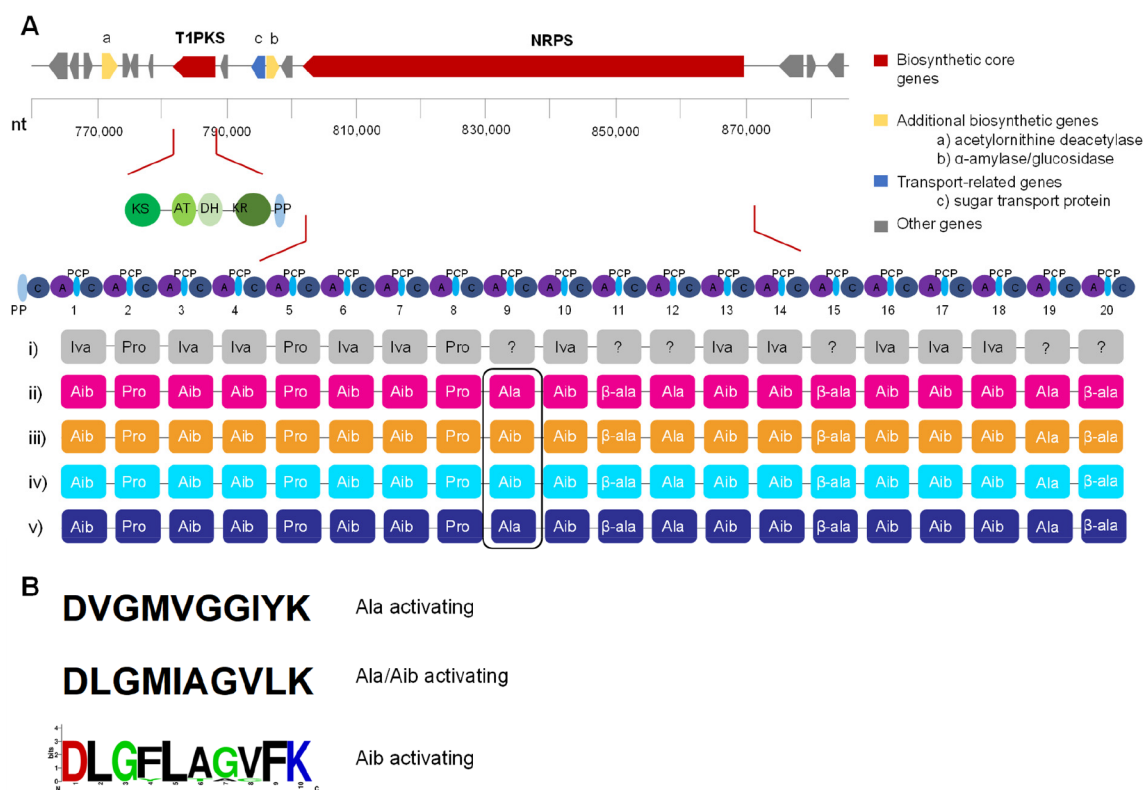


**Figure 7.** (A) Gene organization with open reading frames (ORF) of the putative biosynthetic gene cluster of myropeptins from *M. inundatum* CBS 120646. Domain structures of the type I-polyketide synthase (T1PKS module consists of a beta-ketoacyl synthase (KS), acyltransferase (AT), dehydratase (DH), ketoreductase (KR), and phosphopantetheine acyl carrier protein group (PP)) and the 20-module nonribosomal peptide synthetase (NRPS, modules consist of condensation (C), adenylation (A), and peptidyl-carrier protein (PCP) domains) are shown. (i) The fungiSMASH prediction of loaded substrates (Iva = isovaline, Pro = proline, ? = no consensus), (ii–v) The observed loaded substrates experimentally found for myropeptin C (ii), D (iii), E (iv), and A<sub>1</sub> (v). (B) Stachelhaus specificity codes from A domains responsible for Ala loading (top row), Aib loading (bottom row), and loading of both Ala and Aib (middle row); bottom motif was generated with WebLogo3.<sup>17</sup>

**Table 4. Minimum Inhibitory Concentration (MIC) Assessment of Lipopeptides 1–4 against the Pathogens *S. aureus* and *C. auris* in  $\mu\text{g/mL}$  (microbroth dilution assay)<sup>a</sup>**

	<i>S. aureus</i> ATCC 25923	<i>S. aureus</i> ATCC BAA-41 (methicillin resistant)	<i>S. aureus</i> ATCC BAA-44 (multidrug resistant)	<i>C. auris</i> CDCB11903
myropeptin C (1)	16	16	16	16
myropeptin D (2)	16	16	16	16
myropeptin E (3)	4	8	8	16
myropeptin A <sub>1</sub> (4)	4	4	4	4
kanamycin	1			
vancomycin		1	1	
caspofungin				2

<sup>a</sup>Kanamycin, vancomycin, and caspofungin were used as positive controls, respectively.

Biodiversity Centre (CBS, Utrecht, The Netherlands). The strain was maintained on slants of oatmeal agar at 4 °C. A seed culture was prepared on SYP-SW agar to serve for three-point inoculation of 130 agar SYP-SW agar plates. The SYP-SW medium contained 10 g/L starch (modified soluble, Fisher Scientific, Waltham, MA, USA), 4 g/L yeast extract (CRITERION, Hardy Diagnostics, VWR, Radnor, PA, USA), 2 g/L peptone (Fisher Scientific), 33.3 g/L instant ocean, and 15 g/L agar (VWR) and was autoclaved at 121 °C for 15 min; 100 × 15 mm Petri dishes were purchased from Fisher Scientific. Inoculated agar plates were incubated for 21 days at 26 °C in an incubator under saturated humidity.

**Extraction and Isolation.** After 21 days of incubation, the agar plates (80) were extracted with EtOAc (VWR) by shaking on a laboratory shaker overnight at 110 rpm and filtered through cheesecloth (3×). The extracts were combined and concentrated *in vacuo* to obtain the organic extract (2.5 g). Next, solid phase extraction (SPE) was applied by using Chromabond C<sub>18</sub> ec columns (10 g, 70 mL, Macherey-Nagel, Dueren, Germany). After equilibrating the solid phase, the organic extract was dissolved in water and loaded on the column, and remaining salt from extraction was removed by washing with water. Then, elution was started by applying a MeCN/H<sub>2</sub>O gradient from 10% to 100%. The myropeptins eluted with 70–80% MeCN, MeCN was evaporated, and the remaining water was lyophilized to preconcentrate the fractions. Finally, semipreparative HPLC-UV (210 nm) with a MeCN/H<sub>2</sub>O gradient from 60% to 100% over a Kinetex C<sub>18</sub> column (125 × 10 mm, 5  $\mu\text{m}$ , Phenomenex) and a flow rate of 4 mL/min separated the final, purified lipopeptides. Myropeptins were isolated as white amorphous powders at the following retention times and yields: 1, 5 min, 10 mg; 2, 7 min, 4 mg; 3, 9 min, 30 mg; 4, 13 min, 2 mg (after repurification, lipophilic impurities after the first semipreparative step).

**Determination of Absolute Configuration of Amino Acids: Marfey's Analysis.** Amino acid configurations of lipopeptides 1–4 were determined by acid hydrolysis and subsequent derivatization with Marfey's reagent (1-fluoro-2,4-dinitrophenyl-5-L-alanine amide, L-FDAA, Thermo Fisher Scientific).<sup>31</sup> In order to perform coelution experiments with L-FDAA-derivatized amino acid standards, a slightly modified method based on Sica et al. was used.<sup>32</sup> Briefly, 0.8–1.0 mg of isolated lipopeptides was dissolved in 500  $\mu\text{L}$  of 6 N HCl in a 2 mL glass vial and heated at 110 °C for 24 h. The solution was lyophilized, and the dried hydrolysate was resuspended in 25  $\mu\text{L}$  of H<sub>2</sub>O, 10  $\mu\text{L}$  of

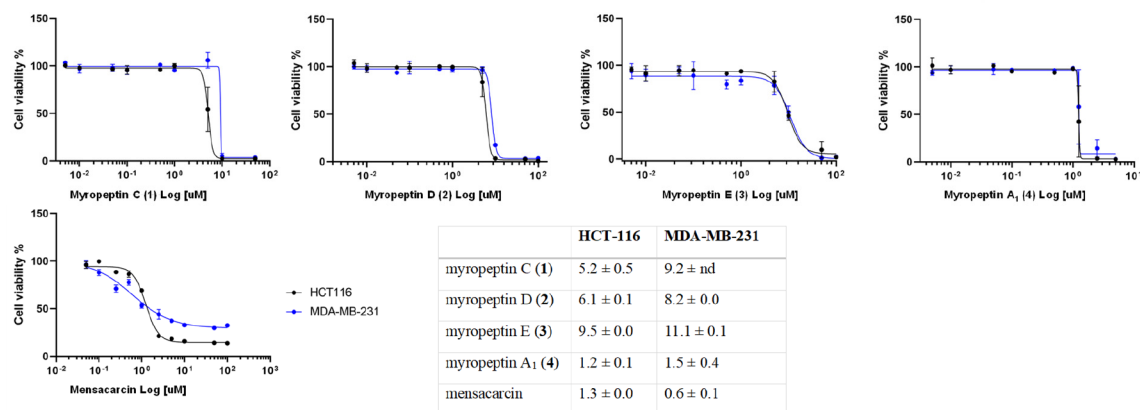


**Figure 8.** Concentration–response curves for the antiproliferative effects of myropeptins 1–4 and mensacarcin as positive control in HCT116: human colon carcinoma and MDA-MB-231: human breast cancer after 24 h. Results represent biological triplicates and two technical replicates as mean ± SEM. Corresponding antiproliferative effects [ $\mu\text{M}$ ] of myropeptins 1–4 and control mensacarcin against cancer cell lines in an MTT assay after 24 h,  $\pm\text{nd}$  = could not be determined by GraphPad Prism due to the high slope factor and no data points in the steepest part of the dose–response curve.

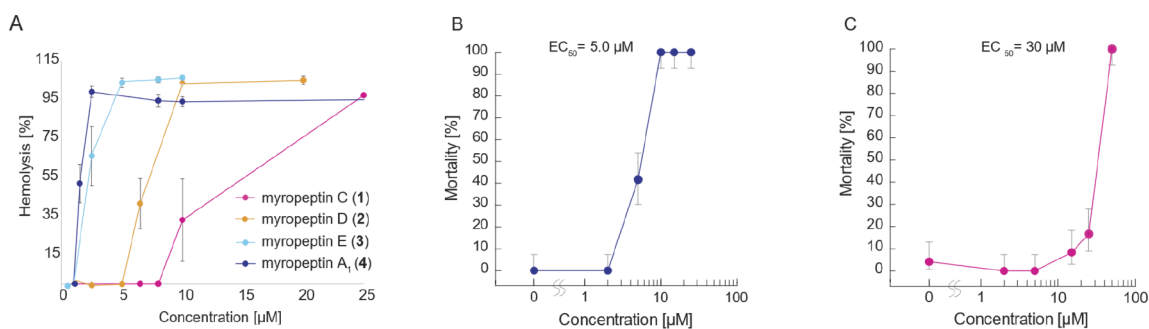


**Figure 9.** (A) Hemolytic activities of lipopeptides 1–4. Sheep erythrocytes were incubated with different concentrations at 37 °C for 1 h, and  $\text{OD}_{450}$  was measured. Data are the average of three independent experiments. Error bars represent the standard deviations. (B, C) Effects of 4 and 1 on zebrafish embryo mortality at concentrations of 2–25  $\mu\text{M}$  (8 embryos, 72 h post-fertilization (hpf) per concentration).

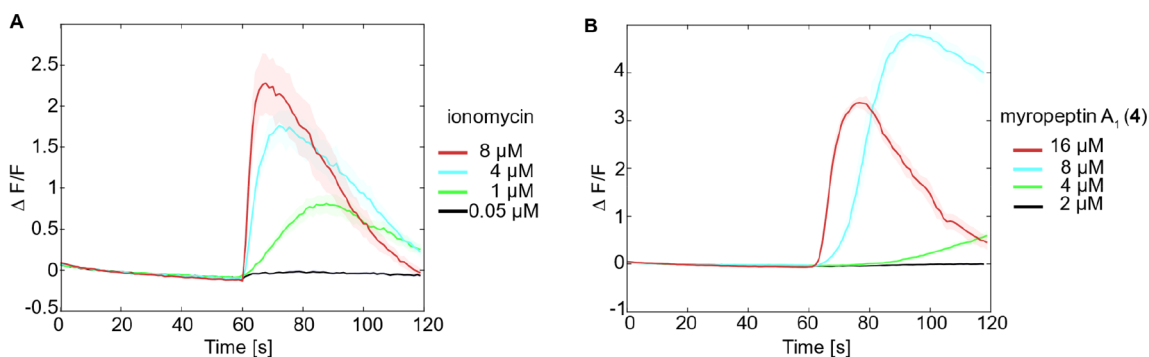


**Figure 10.** (A) Fluo-4 fluorescence changes ( $\text{Ca}^{2+}$ -influx) in SK-Mel-5 cells after perfusion of cells with ionomycin and (B) myropeptin A<sub>1</sub> (4). 60 s of no perfusion (baseline recording), then 30 s of perfusion with respective compound treatment solution ( $\mu\text{M}$ , in 1× PBS, with 0.5% DMSO, 1 mM  $\text{CaCl}_2$ , and 1 mM  $\text{MgCl}_2$ ), followed by 30 s of recording,  $n = 3$ ; shaded areas indicate bootstrap standard error.

aqueous  $\text{NaHCO}_3$  (1 M), and 50  $\mu\text{L}$  of L-FDAA (1% w/v in acetone) and stirred at 40 °C for 1 h. Then, the reaction was quenched with 5  $\mu\text{L}$  of HCl (2 N), and the solutions were lyophilized and prepared for LC-DAD-HRMS analysis by dissolving in MeCN and dilution of 1:10 under starting conditions (10% MeCN + 0.1% FA). Amino acid standards (0.2–0.3 mg of L-alanine, D-alanine,  $\beta$ -alanine, L-proline, D-proline, and  $\alpha$ -aminoisobutyric acid, all Fisher Scientific) were prepared in 50  $\mu\text{L}$  of  $\text{H}_2\text{O}$ , 20  $\mu\text{L}$  of  $\text{NaHCO}_3$  (1 M), and 100  $\mu\text{L}$  of L-FDAA (1% w/v in acetone) and stirred at 40 °C for 1 h. The lyophilized reaction mixture was dissolved, as described above, and analyzed by high-resolution LC-MS.

**Myropeptin C (1):** white amorphous solid;  $[\alpha]_D^{20} +4.6$  ( $c$  0.8, MeOH); HRMS (ESI)  $m/z$  911.5476,  $[\text{M} - 2\text{H}]^{2-}$  calcd for  $\text{C}_{87}\text{H}_{148}\text{N}_{20}\text{O}_{22}$ , 911.5466;  $^1\text{H}$  and  $^{13}\text{C}$  NMR, cf. Table 1; UV/vis (MeCN)  $\lambda_{\text{max}} = 210$  nm.

**Myropeptin D (2):** white amorphous solid;  $[\alpha]_D^{20} +3.1$  ( $c$  0.2, MeOH); HRMS (ESI)  $m/z$  918.5544,  $[\text{M} - 2\text{H}]^{2-}$  calcd for  $\text{C}_{88}\text{H}_{150}\text{N}_{20}\text{O}_{22}$ , 918.5544;  $^1\text{H}$  and  $^{13}\text{C}$  NMR, cf. Table 2; UV/vis (MeCN)  $\lambda_{\text{max}} = 210$  nm.

**Myropeptin E (3):** white amorphous solid;  $[\alpha]_D^{20} +13.0$  ( $c$  0.4, MeOH); HRMS (ESI)  $m/z$  932.5701,  $[\text{M} - 2\text{H}]^{2-}$  calcd for  $\text{C}_{90}\text{H}_{154}\text{N}_{20}\text{O}_{22}$ , 932.5701;  $^1\text{H}$  and  $^{13}\text{C}$  NMR, cf. Table 3; UV/vis (MeCN)  $\lambda_{\text{max}} = 210$  nm.

**Myropeptin A<sub>1</sub> (4):** white amorphous solid;  $[\alpha]_D^{20} +15.5$  (c 1.2, MeOH); HRMS (ESI)  $m/z$  925.5632,  $[M - 2H]^{2-}$  calcd for C<sub>89</sub>H<sub>152</sub>N<sub>20</sub>O<sub>22</sub>, 925.5622; <sup>1</sup>H and <sup>13</sup>C NMR, cf. Table S2; UV/vis (MeCN)  $\lambda_{max} = 210$  nm.

**Cell Culture Assays.** Colon cancer cells (HCT-116) were purchased from the American Type Culture Collection (ATCC, Manassas, VA, USA). Melanoma cells (SK-Mel-5) were obtained from the National Cancer Institute (NCI) cell line repository (Frederick, MD, USA). Triple-negative breast cancer cells (MDA-MB-231) were a kind gift from Dr. April Risinger (UTHSCSA). Dulbecco's modified Eagle's medium (DMEM), phosphate buffer saline (PBS), trypsin/EDTA (0.25%/2.21 mM), and penicillin/streptomycin solution were obtained from Thermo Fisher Scientific. Fetal bovine serum (FBS) was obtained from R&D Systems.

HCT-116, SK-Mel-5, and MD-MB-231 cells were cultivated in DMEM, each supplemented with 10% (v/v) FBS, penicillin (100 U/mL), and streptomycin (100  $\mu$ g/mL). The cell lines were incubated at 37 °C, 5% CO<sub>2</sub>. Cells were plated into 96-well plates at different densities (HCT-116: 7000 cells/well; SK-Mel-5: 6000 cells/well; MDA-MB-231: 8000 cells/well). The passage number for cells used in the experiments never exceeded 15. All cell lines tested mycoplasma-negative by real-time PCR (Myco Solutions mycoplasma detection kit, Akron Biotech, Boca Raton, FL, USA).

Growth inhibition and cytotoxicity in the different cell lines were measured by the reduction of the tetrazolium salt MTT in metabolically active cells. Cells were plated into 96-well plates and maintained overnight before treatment was started with the addition of test compound to each well. After the designated time, MTT (5 mg/mL in PBS) was added to each well at a final concentration of 0.5 mg/mL. The plates were incubated for 2 h at 37 °C. The medium was removed, cells were lysed, and the purple formazan product was solubilized by the addition of 50  $\mu$ L of DMSO. Absorbance was measured at 550 nm with a microplate reader (Synergy HTX, Biotek, Winooski, VT, USA). Metabolic activity of vehicle-treated cells (0.5% DMSO unless otherwise stated) was defined as 100% cell growth.

**Antimicrobial Assays.** For antibacterial activity in cell-based assays, established protocols were followed.<sup>33,34</sup> Gram-positive bacteria, including *Enterococcus faecium* (ATCC 49032), *Staphylococcus aureus* (ATCC 25923), methicillin-resistant *Staphylococcus aureus* (ATCC BAA-41), and multidrug-resistant *Staphylococcus aureus* (ATCC BAA-44), as well as two Gram-negative pathogens, *Pseudomonas aeruginosa* (ATCC 15442) and *Escherichia coli* (ATCC 8739), and *Candida auris* (CDC B11903) were tested. Vancomycin, kanamycin, ampicillin, and caspofungin were used as positive controls. DMSO served as the negative control. For the single-dose assay, compounds, mixtures, and antibiotic controls were tested at 125  $\mu$ g/mL. Microbial growth rates were measured after 16 h by absorbance at 620 nm using a Biotek Synergy 96-well plate reader. All human pathogens used in the study were acquired from the ATCC.

**Hemolysis Assay.** Hemolytic activity was determined using defibrinated sheep blood (VWR). One milliliter of blood was washed 3 $\times$  with PBS (1 $\times$ ) by gentle vortexing, followed by a centrifuge step at 4000 rpm for 5 min and discarding of the supernatant. The remaining cells were diluted (1:500) to achieve  $\sim 8 \times 10^7$  cells/mL. 0.1% Triton X-100 (Fisher Scientific) served as a positive control. Lipopeptide 1–4 stock solutions were prepared in 20-fold concentrations in PBS (1 $\times$ ) + 0.5% DMSO. Then, 190  $\mu$ L of blood suspension and 10  $\mu$ L of sample stock solutions were mixed and incubated for 1 h at 37 °C. Subsequently, the samples were centrifuged at 4000 rpm for 5 min, and 100  $\mu$ L of the supernatant was transferred to a 96-well plate. OD<sub>450</sub> was determined with a microplate reader (Synergy HTX, Biotek).

**Zebrafish Assay: In Vivo Toxicity.** Zebrafish adults (*Danio rerio*, AB strain) were reared under standard conditions (28 °C, 14:10 light:dark) and crossed to produce embryos. Embryos with intact chorions were transferred into 96-well plates (1 embryo/well) at 24 h postfertilization (hpf) using 50  $\mu$ L of medium (HEPES-buffered E3: 5 mM NaCl, 0.17 mM KCl, 0.33 mM CaCl<sub>2</sub>, 0.33 mM MgSO<sub>4</sub>, 1 mM HEPES, titrated to 7.2 pH). Myropeptins C (1) and A<sub>1</sub> (4) were dissolved in DMSO, serially diluted using HEPES-buffered E3, and

then added to well plates (final conc for 1: 0, 2.0, 5.0, 15, 25, and 50  $\mu$ M in 1% DMSO; final conc for 4: 0, 2.0, 5.0, 10, 15, and 25  $\mu$ M in 1% DMSO; total volume in each well: 150  $\mu$ L). Plates were incubated for 48 h (72 hpf; 28 °C, 14:10 light:dark), after which the number of surviving embryos was counted. Each assay examined 8 embryos per concentration, and the assay was replicated 3 times using animals from 3 clutches. The results were similar across replicates, and so survivorship is plotted from pooled data, with error bars representing 68% confidence intervals (like SEM) found by fitting results for each concentration to a binomial distribution (MATLAB R2020b). EC<sub>50</sub> values were calculated by fitting unpooled survivorship values to the Hill equation, and 95% confidence intervals were calculated using a bootstrap analysis. Protocols were approved by the University of Florida's Institutional Animal Care and Use Committee.

**Fluo-4-AM Assay for Ca<sup>2+</sup>-Influx.** SK-Mel-5 cells were cultured as described in the cell culture section, and 20,000 cells/well were seeded in a black 96-well glass-bottom plate overnight. After removing the medium, cells were incubated in the calcium indicator Fluo-4 AM (Invitrogen, Thermo Fisher Scientific; 100  $\mu$ L of 3.5  $\mu$ M Fluo-4 AM in 1 $\times$  PBS supplemented with 1 mM CaCl<sub>2</sub>, 1 mM MgCl<sub>2</sub>, 0.025% DMSO, and 0.005% Pluronic F-127) for 30 min at 37 °C in the dark. The dye loading solution was removed, and then cells were washed with buffer and left in the buffer (100  $\mu$ L of 1 $\times$  PBS with 1 mM CaCl<sub>2</sub> and 1 mM MgCl<sub>2</sub>). Cells were imaged using epifluorescence microscopy (Olympus IX71, objective: 20 $\times$ /0.45 LUCPlanFLN, camera: Hamamatsu C10600-10B-H [0.9 frame/s, 1 s exposure], light: Sutter LB-LS/17, excitation: 482/35 nm with 1.0 ND filter, emission: 536/40 nm). Baseline fluorescence was recorded for 30 s; then test compounds were perfused directly onto cells for 30 s using a rapid solution changer (BioLogic RSC-160). Then the fluorescence was recorded for an additional 30 s. Test compounds included myropeptin A<sub>1</sub> (4) at 2.0, 4.0, 8.0, and 16  $\mu$ M in buffer. Ionomycin (Cayman Chemicals, Ann Arbor, MI, USA) was used as a positive control and was examined at 0.050, 1.0, 4.0, and 8.0  $\mu$ M in buffer with 0.5% DMSO. All experiments were run in triplicates. Responses were analyzed by manually drawing regions of interest around cells, and the  $\Delta F/F$  for individual cells was computed by subtracting background fluorescence then calculating the difference between the instantaneous fluorescence and baseline fluorescence, normalized by the baseline fluorescence. Responses were similar between replicates, so recordings from all cells were pooled, and the results are presented using robust statistics (median  $\pm$  SEM, where the SEM is estimated using a bootstrap analysis).

**Confocal Microscopy.** MitoOrange CMTMRos (ABP Biosciences, Beltsville, MD, USA) was purchased in 1 mg/mL DMSO. A working solution was made fresh from stock prior to the experiments at 200  $\mu$ M in PBS (1 $\times$ ). Coverslips (VWR, Radnor, PA, USA) were washed with 70% ethanol, dried, and coated with 0.1% poly-L-lysine solution (Fisher Scientific). After incubation of 4 h, the coating solution was removed and slips were rinsed with sterile water, dried, and sterilized under UV light for 15 min. Coated coverslips were then placed into a six-well plate, and no more than  $\sim 1 \times 10^6$  cells/cm<sup>2</sup> were seeded onto the coverslip surface. Cells were incubated at 37 °C, 5% CO<sub>2</sub>, before treatment. After 24 h, the medium was removed, and cells were washed once with warm PBS (1 $\times$ ). Then, 1 mL of treatment solution was added, containing a final concentration of 2  $\mu$ M MitoOrange, 0.1% Hoechst 33342, and either 0.1% DMSO (control), 50  $\mu$ M FCCP (positive control), or 1  $\mu$ M myropeptin A<sub>1</sub> (4). The incubation time was 30 min at 37 °C and 5% CO<sub>2</sub>. Afterward, the solution was removed, and cells were washed twice with warm PBS (1 $\times$ , 1 mM CaCl<sub>2</sub>, MgCl<sub>2</sub>). The slip was mounted on a glass microscope slide, and cells were imaged with a Zeiss LSM 710 confocal microscope using a 20 $\times$  objective and transmission light, MitoOrange CMTMRos, and Hoechst 33342 filter sets.

**Flow Cytometry Analysis.** For detection of apoptosis, a kit was used according to the manufacturer's instructions (annexin V apoptosis detection kit I, BD Biosciences, San Diego, CA, USA). Melanoma (SK-Mel-5) cells were seeded ( $1 \times 10^6$  cells) in T25 culture flasks. After 24 h of incubation (37 °C, 5% CO<sub>2</sub>), the medium was removed, and cells were treated with controls and myropeptin A<sub>1</sub>

(4, 1 and 4  $\mu\text{M}$ ) for 3 h. Treatment solutions were prepared in cell medium, and 0.5% DMSO served as a negative control (vehicle) and 5  $\mu\text{M}$  camptothecin as positive control for early apoptosis. After cells were detached ( $\sim 1.5 \times 10^6$  cells) from each T25 flask after trypsin treatment, they were centrifuged at 700g, 3 min, RT. The obtained cell pellet was washed with PBS (1 $\times$ ), resuspended in 1 mL of annexin V binding buffer (1 $\times$ ), and gently mixed. A 100  $\mu\text{L}$  amount of the latter solution was transferred to a new sample tube, and 5  $\mu\text{L}$  of propidium iodide and 5  $\mu\text{L}$  of FITC annexin V were added and incubated for 15 min at RT in the dark. Afterward, 400  $\mu\text{L}$  of annexin V binding buffer (1 $\times$ ) was added to each tube, and samples were analyzed with a BD FACSMelody (BD Biosciences, San Diego, CA, USA) within 1 h. A total of 20,000 events were recorded for each sample, and the BD FACSChorus software was used.

## ■ ASSOCIATED CONTENT

### SI Supporting Information

The Supporting Information is available free of charge at <https://pubs.acs.org/doi/10.1021/acs.jnatprod.3c00148>.

Processing steps, extracted ion chromatograms, and spectra of compounds (PDF)

## ■ AUTHOR INFORMATION

### Corresponding Author

Sandra Loesgen – Department of Chemistry, Whitney Laboratory for Marine Bioscience, University of Florida, St. Augustine, Florida 32080, United States; [orcid.org/0000-0003-1090-564X](https://orcid.org/0000-0003-1090-564X); Email: [sandra.loesgen@ufl.edu](mailto:sandra.loesgen@ufl.edu)

### Authors

Annika Jagels – Department of Chemistry, Whitney Laboratory for Marine Bioscience, University of Florida, St. Augustine, Florida 32080, United States

Donovan A. Adressa – Loxo Oncology, Louisville, Colorado 80027, United States

Elizabeth N. Kaweesa – Department of Chemistry, Whitney Laboratory for Marine Bioscience, University of Florida, St. Augustine, Florida 32080, United States

Mark McCauley – Department of Chemistry, Whitney Laboratory for Marine Bioscience, University of Florida, St. Augustine, Florida 32080, United States

Benjamin Philmus – Department of Pharmaceutical Sciences, Oregon State University, Corvallis, Oregon 97331, United States; [orcid.org/0000-0003-2085-0873](https://orcid.org/0000-0003-2085-0873)

James A. Strother – Department of Biology, Whitney Laboratory for Marine Bioscience, University of Florida, St. Augustine, Florida 32080, United States

Complete contact information is available at: <https://pubs.acs.org/10.1021/acs.jnatprod.3c00148>

### Notes

The authors declare no competing financial interest.

## ■ ACKNOWLEDGMENTS

We wish to thank James Rocca for excellent NMR support. NMR spectra for compound 3 were acquired using a unique 1.5 mm high temperature superconducting cryogenic probe at the McKnight Brain Institute, the National High Magnetic Field Laboratory's Advanced Magnetic Resonance Imaging and Spectroscopy (AMRIS) Facility, which is supported by National Science Foundation Cooperative Agreement DMR-1644779 and the State of Florida. We thank Prof. Dr. Christine Schnitzler and Dr. Danielle de Jong for support with flow

cytometric analysis and confocal microscopy. We also acknowledge Amelia Bunnell for help with zebrafish care. This work was supported by NSF CH-2020110 (S.L.) and German Research Foundation, DFG project number 452319713 (A.J.). S.L. is grateful for UF Start-Up funds.

## ■ REFERENCES

- (1) Lombard, L.; Houbraken, J.; Decock, C.; Samson, R. A.; Meijer, M.; Reblova, M.; Groenewald, J. Z.; Crous, P. W. *Persoonia* **2016**, *36*, 156–246.
- (2) Chen, Y. *Mycosphere* **2016**, *7* (1), 64–80.
- (3) Basnet, B. B.; Liu, L.; Chen, B.; Suleimen, Y. M.; Yu, H.; Guo, S.; Bao, L.; Ren, J.; Liu, H. *Planta Med.* **2019**, *85* (9–10), 701–707.
- (4) Nordberg, H.; Cantor, M.; Dusheyko, S.; Hua, S.; Poliakov, A.; Shabalov, I.; Smirnova, T.; Grigoriev, I. V.; Dubchak, I. *Nucleic Acids Res.* **2014**, *42*, D26–31.
- (5) Hertweck, C. *Nat. Chem. Biol.* **2009**, *5* (7), 450–2.
- (6) Frisvad, J. C. *Methods Mol. Biol.* **2012**, *944*, 47–58.
- (7) Bode, H. B.; Bethe, B.; Hofs, R.; Zeec, A. *ChemBiochem* **2002**, *3* (7), 619–27.
- (8) Marmann, A.; Aly, A. H.; Lin, W. H.; Wang, B. G.; Proksch, P. *Mar. Drugs* **2014**, *12* (2), 1043–1065.
- (9) Yoshimura, A.; Nishimura, S.; Suzuki, T.; Hattori, A.; Dohmae, N.; Kato, T.; Kakeya, H. *Org. Lett.* **2019**, *21* (18), 7524–7528.
- (10) Bhushan, R.; Brückner, H. J. *Amino Acids* **2004**, *27* (3), 231–247.
- (11) Siemion, I. Z.; Wieland, T.; Pook, K. H. *Angew. Chem., Int. Ed. Engl.* **1975**, *10*, 702–3.
- (12) Karle, I. L.; Balaram, P. *Biochem.* **1990**, *29* (29), 6747–6756.
- (13) Wada, S.; Urase, T.; Hasegawa, Y.; Ban, K.; Sudani, A.; Kawai, Y.; Hayashi, J.; Urata, H. *Bioorg. Med. Chem.* **2014**, *22* (24), 6776–80.
- (14) Du, L.; Risinger, A. L.; Mitchell, C. A.; You, J.; Stamps, B. W.; Pan, N.; King, J. B.; Bopassa, J. C.; Judge, S. I. V.; Yang, Z.; Stevenson, B. S.; Cichewicz, R. H. *Proc. Natl. Acad. Sci. U S A* **2017**, *114* (43), E8957–E8966.
- (15) Toniolo, C.; Polese, A.; Formaggio, F.; Crisma, M.; Kamphuis, J. J. *Am. Chem. Soc.* **1996**, *118* (11), 2744–2745.
- (16) Blin, K.; Shaw, S.; Steinke, K.; Villebro, R.; Ziemert, N.; Lee, S. Y.; Medema, M. H.; Weber, T. *Nucleic Acids Res.* **2019**, *47* (W1), W81–W87.
- (17) Crooks, G. E.; Hon, G.; Chandonia, J. M.; Brenner, S. E. *Genome Res.* **2004**, *14* (6), 1188–90.
- (18) Hai, Y.; Jenner, M.; Tang, Y. *J. Am. Chem. Soc.* **2019**, *141* (41), 16222–16226.
- (19) Little, R. F.; Hertweck, C. *Nat. Prod. Rep.* **2022**, *39* (1), 163–205.
- (20) Stachelhaus, T.; Mootz, H. D.; Marahiel, M. A. *Chem. Biol.* **1999**, *6* (8), 493–505.
- (21) Challis, G. L.; Ravel, J.; Townsend, C. A. *Chem. Biol.* **2000**, *7* (3), 211–24.
- (22) Rausch, C.; Weber, T.; Kohlbacher, O.; Wohlleben, W.; Huson, D. H. *Nucleic acids Res.* **2005**, *33* (18), 5799–5808.
- (23) Mosmann, T. J. *Methods* **1983**, *65* (1), 55–63.
- (24) Suzuki, Y.; Yokoyama, K. *Biosensors* **2015**, *5* (2), 337–63.
- (25) Green, D. R.; Reed, J. C. *Science* **1998**, *281* (5381), 1309–1312.
- (26) Wlodkowic, D.; Skommer, J.; Darzynkiewicz, Z. *Methods Mol. Biol.* **2009**, *559*, 19–32.
- (27) Chambers, M. C.; Maclean, B.; Burke, R.; Amodei, D.; Ruderman, D. L.; Neumann, S.; Gatto, L.; Fischer, B.; Pratt, B.; Egertson, J.; Hoff, K.; Kessner, D.; Tasman, N.; Shulman, N.; Frewen, B.; Baker, T. A.; Brusniak, M. Y.; Paulse, C.; Creasy, D.; Flashner, L.; Kani, K.; Moulding, C.; Seymour, S. L.; Nuwaysir, L. M.; Lefebvre, B.; Kuhlmann, F.; Roark, J.; Rainer, P.; Detlev, S.; Hemenway, T.; Huhmer, A.; Langridge, J.; Connolly, B.; Chadick, T.; Holly, K.; Eckels, J.; Deutsch, E. W.; Moritz, R. L.; Katz, J. E.; Agus, D. B.; MacCoss, M.; Tabb, D. L.; Mallick, P. *Nat. Biotechnol.* **2012**, *30* (10), 918–20.

- (28) Pluskal, T.; Castillo, S.; Villar-Briones, A.; Oresic, M. *BMC Bioinform.* **2010**, *11*, 395.
- (29) RStudioTeam. *RStudio: Integrated Development for R*; RStudio, PBC, 2020.
- (30) Wickham, H. *ggplot2: Elegant Graphics for Data Analysis*; Springer: New York, NY, 2016.
- (31) Marfey, P. *Carlsberg Res. Commun.* **1984**, *49* (6), 591.
- (32) Sica, V. P.; Rees, E. R.; Raja, H. A.; Rivera-Chávez, J.; Burdette, J. E.; Pearce, C. J.; Oberlies, N. H. *Phytochem.* **2017**, *143*, 45–53.
- (33) Wiegand, I.; Hilpert, K.; Hancock, R. E. *Nat. Protoc.* **2008**, *3* (2), 163–75.
- (34) CLSI. *Performance Standards for Antimicrobial Susceptibility Testing M100*, 30th ed.; Clinical and Laboratory Standards Institute: Wayne, PA, 2020.